JOURNAL OF MATERIALS SCIENCE 39 (2004) 6023–6042

Chemical reactivities of hafnium and its derived boride, carbide and nitride compounds at relatively mild temperature

Y. D. BLUM
SRI International, 333 Ravenswood Ave., Menlo Park, CA 94025, USA
E-mail: yigal.blum@sri.com

H.-J. KLEEBE
Colorado School of Mines, Golden, CO 80401, USA
E-mail: hkleebe@mines.edu

MB_2/SiC composites are materials of choice for ultra-high-temperature structural applications, primarily in the aerospace arena. These composites are processed in a hot-press operation at a temperature range of 1900 to 2200°C. This article assesses potential "mild-temperature" (below 1500°C) chemical reactions that may lead to structures and coatings made of HfB_2/SiC under pressureless or mild-pressure conditions. The reactions are anticipated to be involved in reactive and shape-forming processes, where ceramic precursors and/or reactive powders are incorporated. This article pays special attention to exothermic reactions as well as to formers of a liquid phase; both can aid the desired phase formation, microstructure development, and sintering of the composite under milder conditions than currently practiced. Reactions between loosely mixed powders with melting points significantly above 1500°C were detected by X-ray diffraction (XRD) analyses. Significant solid-phase reactions of the loose powder mixtures were observed at this mild temperature in powder form. Preliminary microstructural studies using scanning electron microscopy (SEM), transmission electron microscopy (TEM), and energy-dispersive X-ray Spectroscopy (EDX) techniques have confirmed the presence of unique reaction mechanisms between the loosely connected particles.

Good examples are the reactions between Hf powder and powders of BN or B_4C, all having melting points above 2200°C, which form at 1500°C, or below HfB_2/HfN and HfB_2/HfC crystalline domains, respectively. These reactions are less intuitive than the reaction with B_2O_3, which forms HfB_2/HfO_2, potentially via molten or gaseous phases of boron oxide.

1. Introduction

1.1. UHTC composites and their processing

The cornerstone of ultra-high-temperature ceramics (UHTCs) is a small group of metal diborides (MB_2, where M = Hf, Zr, Ti) developed over 30 years ago by the U.S. Air Force [1–7]. In those studies, monolithic composites of diborides combined with silicon carbide (ZrB_2/SiC, HfB_2/SiC and ZrB_2/SiC/C) were identified as the baseline UHTCs, because of their enhanced oxidation resistance at high temperature [8, 9]. These composites possess a unique set of material properties including (a) unusually high thermal conductivity, (b) good thermal shock resistance, and (c) modest thermal expansion coefficients that make them particularly well suited for sharp body applications. The composites of ZrB_2/SiC and HfB_2/SiC with volume ratios of 80:20 were found to be particularly efficient UHTCs because the SiC phase enhances the oxidation resistance without adversely affecting other critical properties such as the high-temperature strength [10–12].

The main deficiencies of these composites arise from their high weight and difficulties associated with their extreme processing conditions. Also, to date, their strength and toughness are not as high as desired. Currently, they are fabricated in either billet or plate stock using uniaxial hot-press processing, which requires typical sintering temperatures of 1850 to 2250°C under pressures of 7 to 21 MPa (some of the references report the use of even higher pressures). Typical components processed by hot pressing are axisymmetric, thus requiring significant amounts of machining and cost to fabricate parts such as designed for a leading-edge application. A pressureless process plus the capability to obtain near-net-shape configurations would decrease the component fabrication costs, making these materials more attractive for aerospace applications.

The high density of HfB_2 (10.5 g/cm^3) and, to a lesser extent, ZrB_2 (6.1 g/cm^3), makes them disadvantageous for desirable lightweight aerospace vehicles. Exception to the lightweight rule is the consideration of using these materials as leading-edge materials in future designs of space vehicles. In these designs the heavy leading-edge materials provide the necessary weight counterbalance around the vehicle center to compensate for the heavy mass of the rocket motors at the rear. However, developing the ability to use these composite materials in the form of thick protective coatings (at least 100 μm thick) over lighter materials such as monolithic SiC, SiC/SiC, or C/C composites would be highly desirable for many applications. Such protected structures will also possess higher strength and/or toughness and can be processed under favorable conditions, preferably under pressureless conditions and/or at lower temperatures than currently employed.

It is important to note that the sinterability of hafnium and zirconium borides is not well studied, and most of the current evidence is empirical. Compositions of about $MB_{1.9}$ were found to be more sinterable as well as more resistant to oxidation [13]. Phase diagrams of such metal boride compositions demonstrate a sharp reduction in what is defined as "incipient melting" when the composition of the metal boride is off the M:2B ratio [14, 15]. When the atomic ratio of the Hf to B is 87:13, the melting point of the Hf-B system is minimized at $1880^\circ \pm 15^\circ$C. Also, the unbalanced ratio is expected to increase the defect level, which is required for obtaining high rate diffusivity in solid-solid reactions and sintering.

Understanding the reactive compositions that form intermediate liquid phases or incorporation of *in-situ* exothermic reactions that lead to local melting at the micro scale would lead to improved processability of the desired composites.

1.2. Use of precursors for improved and easier processing

The capability to use precursor technology for triggering relatively low-temperature chemistry to achieve favorable processing conditions or better composite properties can be extrapolated from analyzing the developed microstructures and mechanical properties of hot-pressed samples versus pressureless process samples. For example, a potential approach for using formulations of MB_2 and polymeric precursors to SiC would be a classical one to achieve the desired low-temperature processing. The polymeric precursor can serve as both binder and inter-particle filler that would form homogeneous precipitation of amorphous and, at higher temperature, crystalline silicon carbide around the boride particles.

In addition, the precursors may aid the sinterability of the desired composite. The conventional sinterability of these composites is hampered by the lack of a liquid phase formation, gas species evolution, or phase transformation reactivity at elevated temperature that would enhance the sintering of materials with such high thermal stability. Their sintering must therefore occur via diffusivity in the solid state [16]. This situation requires direct contact between the particulates, which is very inadequate even in a compacted structure, requiring hot press processing of the discussed composites. A precursor that is processed in a liquid form, or forms a liquid phase at an intermediate temperature, can be dispersed around the particulates, thereby forming a large area of contact with the particles and subsequently enhancing the rates of diffusivity. Furthermore, the post-pyrolyzed amorphous intermediate, derived from the polymeric precursor, is metastable and may further react with its surrounding more readily than a crystallized, well-ordered phase of the same material. It can also serve as a high-temperature liquid phase that aids first the sintering and then the formation of the final phases. Sacks *et al.* [17, 18] have demonstrated such a concept in forming mullite materials via "transient viscous sintering." They coated Al_2O_3 particles with a thin silica film that promoted sintering at an intermediate stage before the silica reacts with the alumina to form the desired mullite phase.

Other approaches to activate the MB_2 phase densification at relatively mild conditions can be based on the chemistry of the boride materials or materials that lead to the formation of such borides *in situ*. Such reactions can contribute to the overall phase and microstructure development by leading to thermodynamically favorable phases, being exothermic, or forming a liquid phase to aid sintering and phase transformations.

Therefore, the concept of using "ceramic precursors" is viewed in this study in a broader term that includes:

(a) Polymeric precursors to the desired composite components.
(b) Precursors to intermediate materials that would further interact to form the final product.
(c) Reactive liquid formers as a part of the process.
(d) Reactive powders that would thermodynamically lead to the desired phases during the thermal process.

The concepts for using precursors to MB_2/SiC composites can be divided into two major categories: (a) preceramic polymers to either SiC or metal diboride and (b) powder precursors ("reactive fillers") with favorable reactivity from a thermodynamic standpoint. Additionally, a precursor that leads to a liquid phase intermediate during the thermal cycle would be a plus, provided that the liquid phase is only a small fraction of the entire formulation and no major volume of gas is evolved.

Approaches based on using polymers, precursors to SiC, can (a) generate a better homogeneity between the MB_2 phase and polymer derived SiC moiety, (b) enhance the sinterability of the composite via the chemical activation of the amorphous SiC phase during its crystallization and grain growth activity, and (c) promote chemical interactions between the polymer-derived materials and other particulates in the mixtures such as the metallic forms of Hf, Zr, or Si. A partial proof of concept for using preceramic polymers for the formation of the desired composites has been reported in the patents of Zank from the mid-1990s [19]. In these patents, ZrB_2 powder is mixed with various polymeric precursors to

SiC and heated to between 1900 to 2250°C under pressureless sintering conditions to produce structures with densities of up to 5.56 g/cm^3 (92% of the theoretical 6.08 g/cm^3). These values are quite impressive considering the fact that any polymeric precursor to SiC must shrink to less than 1/3 of its original volume (from a density of about 1 g/cm^3 to 3.1 of SiC) during the process. The patent includes information about the change of density from the green body stage to the pressureless sintered body. For example, a cured green specimen with density of 3.86 g/cm^3 was sintered to a density of 5.56 g/cm^3 in spite of about 5% weight loss during the process. This indicates that a significant densification mechanism occurs in this system under pressureless conditions.

The overall objective of the research reported in this article is to develop the chemistry to assist the formation of HfB_2/SiC composites. Most of the discussion and the experiments described below are geared toward better understanding of the Hf chemistry with other elements and compounds. Due to significant lack of information about the chemistry of Hf and its derivatives, it was necessary to depend on the reported chemistry of the closely related Zr and, to a lesser extent, Ti systems. These two elements have been investigated for their reactivity and high-temperature behavior in much greater depth than has the Hf system [20–22]. Scarcity of Hf, cost, limited applicability (until now), and high-density disadvantage are the prime reasons this element has been studied so little. However, HfB_2- and HfC-based composites are now of high interest as materials for UHTC aerospace applications and are worthy of further study.

2. Experimental

All the powders used in the study were purchased commercially and used as received. Carbon black was purchased from Cabot and boron oxide from Sigma-Aldrich. The rest of the powders were the finest ones available from Cerac. Since all the powders' particle size is based on 325 mesh sieving, further powder characterization has been performed using a Horiba Particle Size Distribution Analyzer—CAPA-700. Table I summarizes the particle size analysis and calculated parameters of the various powders used in the study. The Hf-containing particles were dispersed in Sedisperse A-14 because of their high density. The rest of the powders were dispersed in methanol. Phenolic resin solution (resol) was obtained from Georgia Pacific Company.

TABLE I Analysis of powders used

Type of powder	Size range (μm)	Median diameter (μm)	Standard deviation (μm)	Surface area (m^2/gm)
Boron	0.05–10	0.16	3.52	24.7
Boron carbide	0.05–30	1.11	6.17	5.3
Boron nitride	0.2–8	2.14	1.84	2.5
Carbon black	0.2–9	0.89	2.85	5.3
Hafnium	0.3–20	4.56	5.43	0.2
Hafnium boride	0.3–20	1.78	3.28	0.5
Hafnium carbide	0.3–20	6.18	5.84	0.2
Hafnium nitride	0.2–30	11.62	11.91	0.2
Hafnium oxide	0.1–30	1.45	6.43	1.1
Silicon	0.05–10	5.03	4.72	7.3

Mixtures based on powders only were ball-milled for 16 h in ethanol in polyethylene containers using zirconia balls. Blends, containing soluble precursors, were mixed by first dissolving the precursor in an appropriate solvent, adding the powder, ball-milling the slurry, and removing the solvent by rotor-evaporation to maintain the homogeneity. If necessary, the dried mixture was crushed by mortar and pestle into a powdery form. Pellets were prepared by pressing the mixed powders into a small die (0.5 cm in diameter) at 20 MPa.

A tube furnace furnished with an alumina tube that was sealed and constantly flushed with argon or nitrogen was used for heating the samples. The heating schedule remained standard in all experiments unless otherwise mentioned: heating rate of 5°C/min to either 1000 or 1500°C and a hold time at the maximum temperature for 1 h.

A Phillips XRD apparatus with Cu K_α source and Ge monochromator was used for the powder diffraction analyses. The thermodynamic calculations were performed using HSC Chemistry Version 4.0 software generated by Outokumpu Research Oy, Pori, Finland (1999).

Microstructural characterization of powder samples was performed by SEM using a FEI Quanta600 instrument operating at 30 keV. Prior to imaging, the samples were gold-coated to avoid charging under the electron beam. In addition, TEM was employed using a FEI CM200STEM microscope operated at 200 keV. To minimize charging during TEM imaging and to allow for chemical analysis, the powders, which were placed on a carbon grid with holes, were lightly coated with carbon. Local chemical analysis was performed with a PGT's EDX spectroscopy system with a thin window detector. It should be noted that some of the Hf-containing phases did not reveal distinct intensities of the light elements such as boron, nitrogen, and/or oxygen, due to the rather large thickness of some of the powder particles (extensive absorption by Hf), which made it difficult, if not impossible, to distinguish between HfB_2, HfC, HfN, or HfO_2.

3. Thermodynamic considerations and synthesis/processing guideline

Attempts to develop a rational precursor approach should consider the potential chemistry between elements that can be introduced via polymeric and/or powder precursors and proceed at mild temperature. A literature search for the chemistry of elemental Hf or its boride, carbide, nitride, and even oxide derivatives turned up very little fundamental information; Hf is typically mentioned in conjunction with related studies of other transition metals—Ti and Zr in particular. It was, therefore, critical to initiate this effort by performing experiments involving Hf, its derivatives, and other elements that participate in the HfB_2/SiC system, including incorporation of oxygen and nitrogen due to environmental effects. The early experimental work reported here is dedicated to the screening of potential

chemical reactivity that may occur either in a precursor system or if reactive additives are introduced to ease the conditions for sintering and promote favorable microstructure development. The experiments were based on the following guidelines:

- All the attempted reactions are anticipated to be spontaneous at the designated temperature based on Gibbs' free energy (ΔG) calculations; most are also exothermic, as manifested by negative enthalpy at the reaction temperature (ΔH).
- The reaction temperature is lower than or equal to 1500°C at atmospheric pressure.
- The reactions are set to provide HfB_2 (and SiC at a later stage) at the end of the process.
- Preferably, the reactions are such that the weight loss and gas release at the high-temperature range (beyond pyrolysis) will be minimal. However, release of moderate levels of gas as a result of carbothermal reduction or other reactions is also considered.
- The formation of a fractional liquid-phase intermediate at elevated temperature is advantageous to facilitate the desired phase formation.
- Increasing the contact surface area between reactants would be kinetically beneficial.
- A part of the HfB_2 phase may be developed from a combination of powder precursors or polymeric/powder precursors.

For simplification, the initial screening was performed by mixing the reactants in a form of loosely mixed powders. Pellets were prepared and heated alongside the powders in cases where a liquid phase formation was anticipated during the processing.

Reactions that lead to the formation of HfB_2 are the core of this chemical assessment. Table II lists calculated thermodynamic values of known and anticipated reactions to form HfB_2 that may occur *in situ* as a part of processes involving ceramic precursor concepts.

Table II indicates that most of the reactions involving either metallic Hf or B are exothermic and favorable even at 1000°C. Interestingly, the most common method to form HfB_2—the carbothermal reduction—is very endothermic, although the Gibbs' free energy becomes negative above 1518°C. This reaction leads also to a significant level of gas release, which is unfavorable if it occurs *in situ* during the processing of a structure or a coating with high integrity.

It should be noted that the XRD screening analysis reported in this article serves only as an indicator for the occurrence of reactions that end in a crystalline phase. Therefore, other noncrystalline phases may remain undetectable. Also, the molar ratios between the observed phases cannot be estimated without careful analysis of reference blends of pure crystalline materials. Thus, the extent of reaction completion will require further study.

The most elementary reaction to form HfB_2 is the direct interaction between Hf and B powders. As indicated in Table III, this reaction results in the presence of only HfB_2 phase in the XRD analysis of the 1500°C heated product. This exothermic reaction is a classical candidate for combustion synthesis. Indeed, the synthesis of HfB_2 by self-propagating high-temperature synthesis (SHS) has been reported alongside other diborides, carbides, and nitrides of a series of transition metals [23], and Munir is currently studying the formation of HfB_2 in a condensed composite form using the SHS process [24]. According to a study of Aleksandrov and Korchagin, such reactions between solids involve the melting of the less refractory reactant [25].

Most of the reported carbothermal reductions are based on employing oxides of both the transition metal

TABLE II Calculated thermodynamic values for reactions in which HfB_2 is formed

Reaction	$\Delta G_{1000°C}$ (KJ/mol)	$\Delta H_{1000°C}$ (KJ/mol)	$\Delta G_{1500°C}$ (KJ/mol) (temp of $\Delta G = 0$)	$\Delta H_{1500°C}$ (KJ/mol)
$Hf + 2B = HfB_2$	−315	−328	−308	−332
$Hf + B_2O_3 = HfB_2 + 3/2O_2$	647	901	549	889
$Hf + 2/3B_2O_3 = HfO_2 + 4/3B$	−243	−282	−228	−281
$Hf + 2/5B_2O_3 = 2/5HfB_2 + 3/5HfO_2$	−272	−301	−260	−301
$Hf + B_2O_3 + 3C = HfB_2 + 3CO$	−25	561	−252	538
$Hf + 2BN = HfB_2 + N_2$	−38	171	−119	166
$Hf + BN = HfN + B$	−115	−113	−116	−112
$Hf + 2/3BN = 1/3HfB_2 + 2/3HfN$	−181	−185	−180	−185
$Hf + 1/3B_4C = 2/3HfB_2 + 1/3HfC$	−252	−265	−247	−268
$Hf + 1/2B_4C = HfB_2 + 1/2C$	−278	−296	−270	−298
$Hf + 1/3HfO_2 + 2/3B_4C = 4/3HfB_2 + 2/3CO$	−215	−93	−262	−102
$HfO_2 + 2B = HfB_2 + O_2$	569	774	491	763
$HfO_2 + B_2O_3 + 5C = HfB_2 + 3CO$	410	1435	14 (1518°C)	1398
$HfO_2 + 2B + 2C = HfB_2 + 2CO$	121	546	−43	529
$HfO_2 + 0.5B_4C + 1.5C = HfB_2 + 2CO$	330	608	25 (1580°C)	591
$HfO_2 + 10/3B = HfB_2 + 2/3B_2O_3$	−13	−21	−9	−27
$HfC + 2B = HfB_2 + C$	−113	−124	−108	−126
$HfC + 2B + 2H_2 = HfB_2 + CH_4$	−64	−214	−5	−215
$HfC + 6B = HfB_2 + B_4C$	−171	−191	−163	−196
$HfC + 4/3B + 1/3B_2O_3 = HfB_2 + CO$	−17	172	−89	163
$HfC + 2C + B_2O_3 = HfB_2 + 3CO$	176	765	−51	743
$HfN + 2B = HfB_2 + 1/2N_2$	−61	34	−98	28

TABLE III Reactions between powder mixtures involving the presence of metallic Hf powders

Reactants	Weight change during heating to 1500°C (WT%)	Observed crystalline phases after heating to 1500°C (found by XRD)
Hf + GP Phenolic (calculated for 3 equivalents of C)	−18.2	HfC (very strong) HfO_2 (weak)
H_3BO_3 + GP Phenolic + NH_4OH in water (clear solution)	−28.4	B_2O_3(weak, broad) semi crystallized C (?)
Hf("3C") from AF-2 + $2H_3BO_3$ dissolved in water	−33.3	HfB_2 (very strong) HfO_2 (strong)
Hf + B_2O_3 + 3C (via novolac pyrolysis)	−19.6	HfO_2 (very strong) HfB_2 (strong)
Hf + B	None	HfB_2 (very strong)
Hf + C (carbon black)	+1.2	HfC (very strong)
Hf + B_2O_3 + C (1 h at 1500°C)	−15.5	HfO_2 (very strong) HfB_2 (strong)
Hf + B_2O_3 + C (8 h at 1500°C)	−21.9	HfB_2 (very strong) HfC (strong) HfO_2 (medium)
Hf + B_2O_3	−9.1	HfO_2 (very strong) HfB_2 (strong)
Hf + 2BN	+1.3	HfN (very strong) $Hf_{55}B_{30}N_{10}$ (combined with the HfN picks) HfB_2 (medium) HfO_2 (weak) BN (weak)
Hf + B_4C	+0.1	HfB_2 (very strong) HfC (weak)

and boron as the reactants, such as the following reaction [20]:

$$HfO_2 + B_2O_3 + 5C \longrightarrow HfB_2 + 5CO \qquad (1)$$

However, as shown in Table II, this reaction is very endothermic, even if $\Delta G < 0$ above 1518°C. A modified carbothermal reduction between TiO_2 and B_4C in the presence of excess carbon is actually practiced on a large commercial scale [20, 26, 27], and similar processes were reported for the formation of fine ZrB_2 particles [28]. This reaction is defined as a borothermic/carbothermal reduction:

$$TiO_2 + 0.5B_4C + 1.5C \longrightarrow TiB_2 + 2CO \qquad (2)$$

A similar reaction for the borothermic reduction of HfO_2 would require an even higher temperature to proceed thermodynamically (1580°C), and it is still endothermic, although it requires less energy input than the reaction in Equation 1. Other potential borothermic reductions, which require less energetic conditions (see Table II), are illustrated in Equations 3 and 4:

$$HfO_2 + 2B + 2C \longrightarrow HfB_2 + 2CO \qquad (3)$$

$$HfO_2 + 10/3B \longrightarrow HfB_2 + 2/3B_2O_3 \qquad (4)$$

Reaction (3) is still endothermic, but ΔG is already negative at 1500°C, providing conditions for a spontaneous reaction at this temperature. Reaction (4) is the first in the series of carbothermal and borothermic reductions of HfO_2 to show some exothermic characteristics (see Table II).

4. Results and discussion

4.1. The use of metallic Hf powder as a source for HfB_2 and related compounds

In an attempt to move toward a more exothermic region and reactions with negative ΔG at relatively low temperatures, a series of reactions was performed using metallic Hf instead of the thermodynamically stable HfO_2. These results are summarized in Table III. The reaction between metallic Hf and boron oxide in the presence of carbon forms the desired diboride product at 1500°C:

$$Hf + B_2O_3 + 3C \longrightarrow HfB_2 + 3CO \qquad (5)$$

Although this reaction still requires energy input, its Gibb's free energy value at 1500°C is significantly negative (−252 KJ/mol). Because of the endothermic conditions (positive ΔH), this reaction is relatively slow, as indicated by the mass loss after 1 h of reaction (see Table III), which is about 50% of the loss expected for a complete carbothermal reduction. The XRD profile of the reaction at its intermediate stage is illustrated in Fig. 1a. In general, carbothermal reductions including the reaction of boron oxide are slow because of these endothermic conditions [20]. When the reaction is carried out for 8 h, higher weight loss is detected (see Table III), the XRD pattern of the HfO_2 becomes weaker, and a significant amount of HfC appears as shown in Fig. 1b relative to Fig. 1a.

The SEM image, given in Fig. 2, shows large particles up to 30 μm in size, which are heavily coated with spherical and much smaller particles.

The corresponding TEM image, given in Fig. 3, reveals a larger dark HfB_2 particle (about 500 nm in length) surrounded by much smaller spherical particles (about 10–20 nm in size; see inset), which were identified by EDX as residual carbon.

As shown in the inset, the carbon phase seems to be composed of concentric shells, similar to carbon onions; however, these features are not well crystallized, which is in line with the absence of graphite in the corresponding XRD pattern (Fig. 1a).

It should be mentioned here that there is a discrepancy between the images recorded via SEM and those taken during TEM observations, particularly regarding the particle size observed. This is the result of having used different techniques for powder sampling. Powder specimen preparation for the SEM simply involved directly sampling the original powder and placing it onto a support stub. In contrast, the TEM samples were processed by ultrasonic dispersion of the powder in ethanol and then (after a short period of sedimentation) taking a small volume fraction of the dispersion with a pipette and placing it on a holey carbon grid. Therefore, the powder representation for the TEM study consisted of the very small and/or low density particles

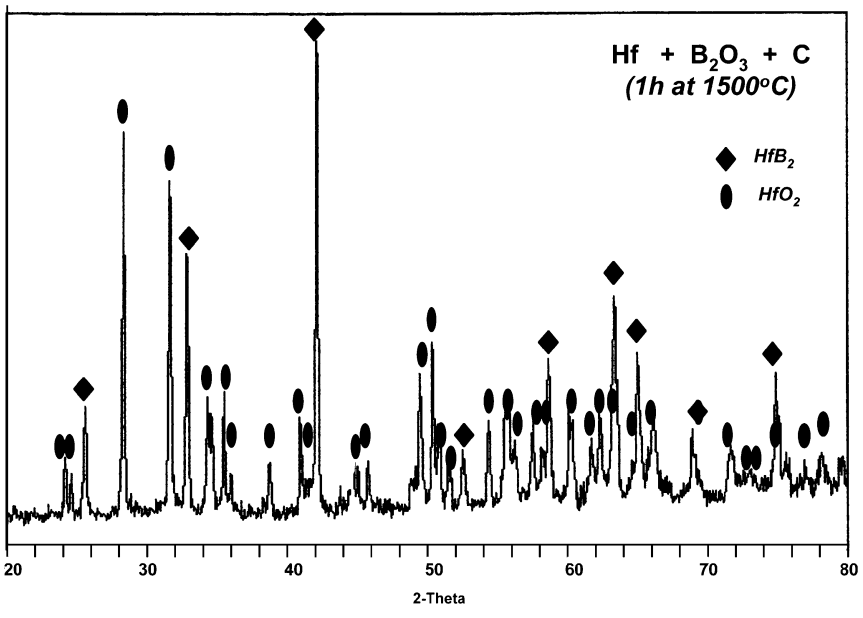

(a)

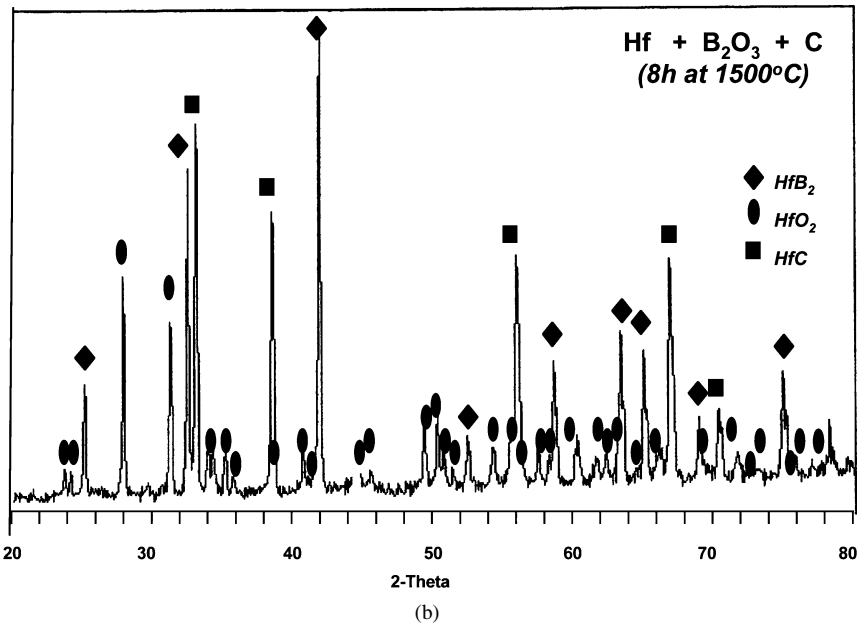

(b)

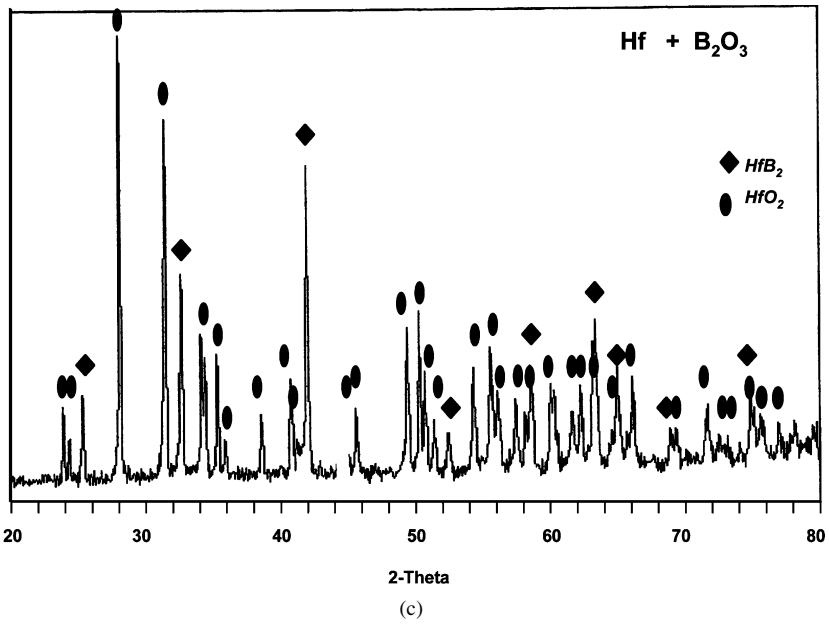

(c)

Figure 1 Reactions between Hf and B_2O_3 (a) in the presence of carbon black reacted at 1500°C for 1 h and (b) for 8 h, (c) in the absence of C, and (d) when a polymeric precursor to carbon (resol) serves as the carbon source. (*Continued on next page*)

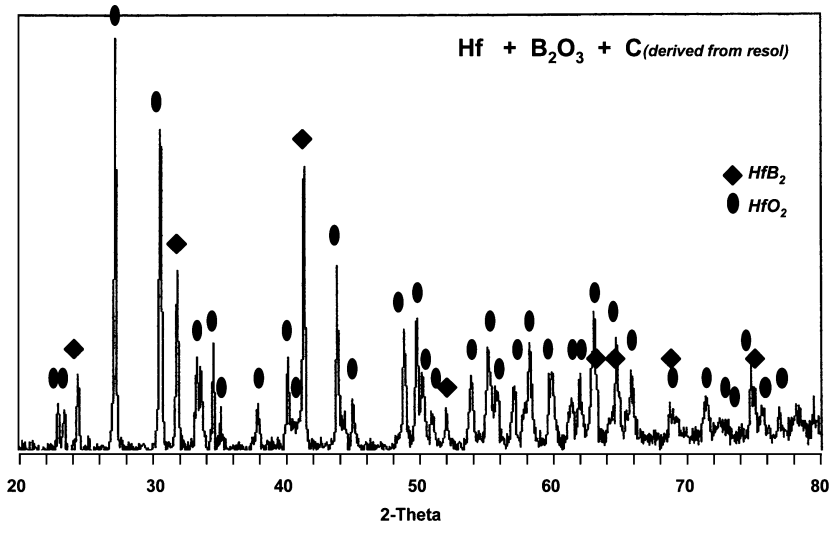

(d)

Figure 1 (*Continued*)

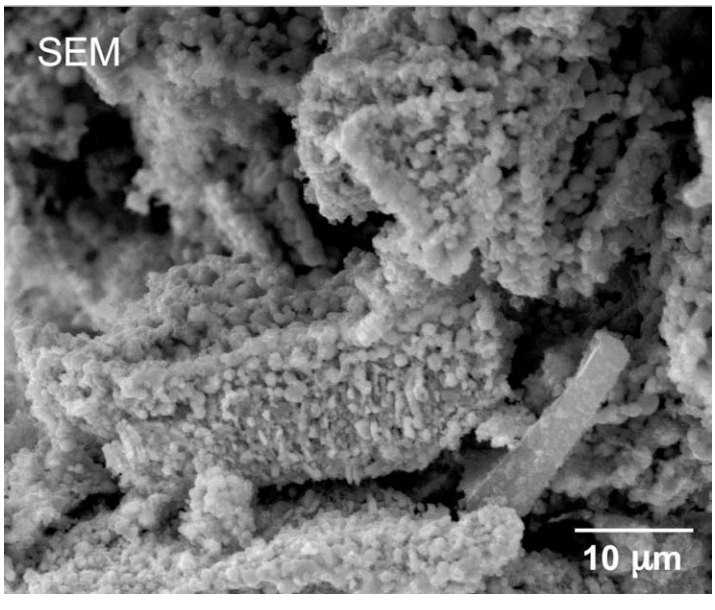

Figure 2 SEM image of the powder sample obtained via reaction (5) at 1500°C, showing rather large particles (up to 30 μm in length) that are coated with much smaller, more spherical particles.

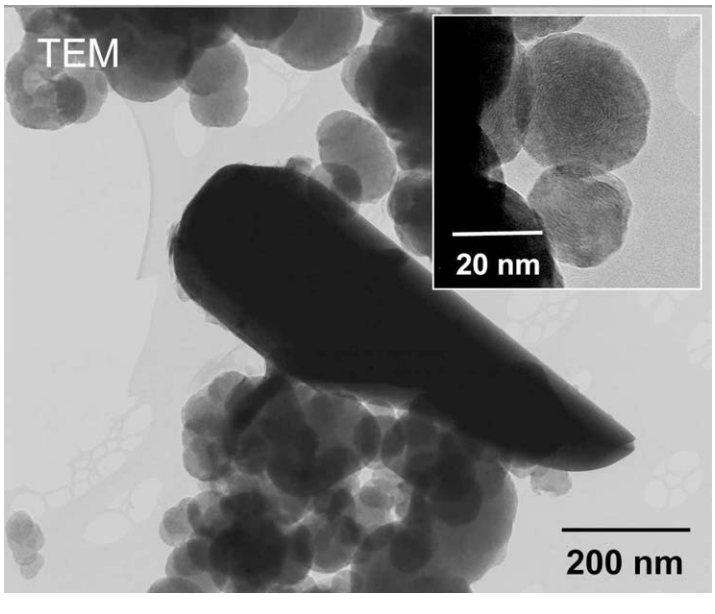

Figure 3 TEM image (corresponding to Fig. 2) that shows an elongated darker particle of HfB_2 in addition to small spherical particles (see also inset), which were identified as carbon spheres (onions).

TABLE IV Thermodynamics of other associated reactions in the system of Hf-B-C-O-N

Reaction	ΔG_{1000} (KJ/mol)	ΔH_{1000} (KJ/mol)	ΔG_{1500} (KJ/mol) (temp of $\Delta G = 0$)	ΔH_{1500} (KJ/mol)
$Hf + C = HfC$	−201	−204	−200	−205
$4B + C = B_4C$	−66	−58	−69	−54
$HfO_2 + 3C = HfC + 2CO$	234	670	66 (1661°C)	655
$2B_2O_3 + 7C = B_4C + 6CO$	520	1711	60 (1561°C)	1669
$Hf + 1/2N_2 = HfN$	−253	−363	−211	−359
$B + 1/2N_2 = BN$	−138	−250	−95	−248
$HfB_2 + 3/2N_2 = HfN + 2BN$	−215	−533	−92	−523
$HfC + 1/2N_2 = HfN + C$	−158	−51	−10	−154

that remained suspended in the solvent. Consequently, the particle size observed in the TEM images is typically much smaller than that observed in the SEM images.

As discussed below, the presence of HfC in the longer-term reaction (8 h) is probably a direct product of the reaction between Hf and C or an intermediate in a stepwise conversion of the evolved HfO_2 via HfC to HfB_2.

The HfO_2 phase suggests that the thermally favorable red-ox reaction between Hf and B_2O_3 occurs during the reaction:

$$Hf + B_2O_3 \longrightarrow HfO_2 + B \qquad (6)$$

This reaction may occur before or in parallel with the carbothermal reduction step, especially because it is exothermic, while the carbothermal reduction of B_2O_3 by itself is still endothermic at 1500°C and $\Delta G = O$ at 1561°C, as shown in Table IV. One possibility is that the Hf is first oxidized by reacting with the B_2O_3 and then reduced by the carbon. Nevertheless, the carbothermal reduction of HfO_2 becomes thermodynamically favored only above 1661°C. Another potential pathway is an initial red-ox reaction followed by carbothermal reduction of the mixed oxide. As shown in Table IV, other reactions are also feasible at 1500°C or below.

To corroborate the presence of a red-ox reaction as a part of the carbothermal reduction, Hf and B_2O_3 were directly reacted without the presence of carbon. Surprisingly, a dissociative-substitution reaction of the boron oxide was observed (Fig. 1c):

$$Hf + 2/5B_2O_3 \longrightarrow 2/5HfB_2 + 3/5HfO_2 \qquad (7)$$

Weight loss associated with this reaction (−9.1 wt%) may be explained either by the release of oxygen, which is not thermodynamically favored according to Table IV, but more likely because of the red-ox reaction associated with the formation of volatile boron oxide and sub-oxide species, which are volatile at the reaction temperature and play a major role in the carbothermal mechanism of B_2O_3 [29].

The SEM image shown in Fig. 4 reveals that the majority of the powder sample contains rather fine, more globular particles (up to 200 nm in diameter). EDX analysis showed that these small particles contained Hf, but a distinction between HfB_2 and HfO_2 could not be made unequivocally.

In addition, lath-like particles with a high aspect ratio were commonly observed throughout the sample. They are most likely HfO_2, but further detailed TEM work to confirm this assumption is in progress. It is rather interesting to note the large variation in particle size and particle morphology, in particular as expressed in the SEM images. Hence, these studies are complementary to the XRD analysis and TEM imaging.

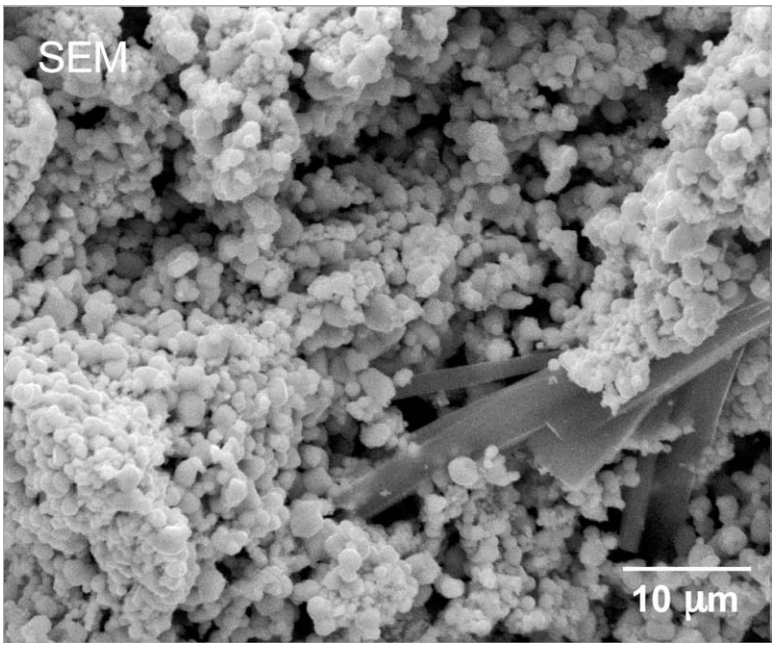

Figure 4 SEM image of the powder sample obtained via reaction (7) at 1500°C, which reveals a distinct variation in particle morphology with a high volume fraction of more globular and some lath-like particles.

Polymeric precursors to carbon would be very attractive as low-cost sources to the carbon needed for carbothermal reductions. They also serve as good binders in processing schemes for MO_2/SiC composite coatings and structures based on polymeric precursor technology. The water-soluble phenol resin, resol, is a convenient candidate as a precursor to carbon because of its commercial availability and previous uses as a carbon source for carbon-carbon composites and even as a reagent to form nanocrystalline ZrC fine powders by solution-based processing [30]. Repeating the reaction in Equation 1 with resol was performed by first mixing Hf powder with resol solution, followed by drying and pyrolysis of the mixture at 800°C (Equation 6). The amount of resol was calculated to provide three equivalents of carbon after pyrolysis. The material was ball-milled, and the resultant powder was mixed with B_2O_3 and heated to 1500°C, as shown in Equations 8 and 9:

$$\text{Hf} + \text{“3 equivalents” Phenolic} \longrightarrow \text{Hf(C)} \quad (8)$$

$$\text{Hf(C)} + B_2O_3 \longrightarrow HfB_2 + 3CO + (HfO_2) \quad (9)$$

The above stepwise approach was taken based on the idea that the formation of carbon as a uniform sealing shell around the Hf particles may serve as a barrier for the direct red-ox reaction discussed above, and allow the formation of HfC as an intermediate, if found to be important in the overall cascade of reactions. The XRD pattern of the powder product is very similar to the one obtained in the reaction with carbon black (Equation 5), as illustrated in Fig. 1d. No HfC phase has been detected in this reaction.

It is tentatively concluded that a polymer-derived carbon can be used in the processing of the desired composites. However, the red-ox reaction has not been suppressed, and it is assumed that cracks and other defects in the polymer-derived shells around the Hf particles allow direct interaction between the B_2O_3 and the metal. Alternatively, the molten B_2O_3 may interact and etch the carbon layer at relatively low temperature. This set of reactions will require further study at a later stage of the research if an efficient formation of HfC as an intermediate is desired.

The Hf(C) powder was also tested for its capability to directly form HfC:

$$\text{Hf(C)} \longrightarrow \text{HfC} \quad (10)$$

This reaction indeed proceeds below 1500°C, and HfC is the only phase detected by XRD analysis. The reaction between Hf and carbon black powder provided a very similar XRD pattern to the one utilizing the polymeric resol source:

$$\text{Hf} + C_{\text{black}} \longrightarrow \text{HfC} \quad (11)$$

These two reactions are expected, since Hf and C are typical reagents for combustion synthesis of such Hf- and carbide-based compounds because of the highly exothermic reactivity ($\Delta H_{1500} = -205$ KJ/mol), as shown in Table III [31]. In comparison, only $\Delta H_{1500} = -54$ KJ/mol is associated with the combustion reaction that forms B_4C from B and C. Comparison of the reactions represented in Equations 10 and 11 at lower temperature or analysis of the derived powders is needed to assess any distinction between the two.

Other potential dissociative reactions between powders have been evaluated. Replacing the B_2O_3 with BN is an intriguing example, because it may lead to either the release of nitrogen (Equation 12) or the dissociative-substitution reaction (Equation 13). Both reactions are feasible based on the calculations shown in Table II.

$$\text{Hf} + 2\text{BN} \longrightarrow HB_2 + N_2 \quad (12)$$

$$\text{Hf} + 2\text{BN} \longrightarrow HfB_2 + \text{HfN} \quad (13)$$

Physically, this reaction must be widely different from the reaction with B_2O_3, since it is expected to be a solid-solid phase reaction between two powdery materials of very high melting point, as the melting point of Hf is 2227°C and solid BN sublimes around 3000°C. Nevertheless, a significant dissociative reaction occurs at 1500°C in a similar manner to the reaction with boron oxide. According to XRD analysis, most of the BN disappears and strong patterns of HfB_2, HfN, and potentially a hafnium boronitride phase, “HfBN,” are observed (see Table II and Fig. 5a):

$$\text{Hf} + 2\text{BN} \longrightarrow HfB_2 + \text{HfN} + \text{“HfBN”} + (HfO_2) \quad (14)$$

The Hf boronitride as well as other boronitrides and carbonitride of transition metals are rarely reported, and typically obtained by performing SHS reactions between metals and B or C in the presence of nitrogen or a metal nitride of the same element [32]. A weak pattern of HfO_2 observed in the XRD profile suggests that small amounts of oxygen were present at the surface of the original powder reactants or potentially scavenged by reactions with the alumina boat and furnace tube or oxygen impurities in the gaseous environment. A weight gain of 1.2 wt% has been detected in this reaction. The presence of oxygen can potentially aid the overall reactivity if, for example, BO_x species, including liquid B_2O_3 and gaseous species, are formed as intermediates in the reducing environment. Such species are postulated as the vehicle for forming carbides and borides under carbothermal reaction conditions [29, 33].

The SEM image representing reaction (14) shows rather large particles, many of which are plate-like in nature (Fig. 6). No fine spherical particles are observed in this SEM sample. Again, a clear distinction between HfB_2 and HfN (or HfBN) could not be detected by EDX analysis (due to the large penetration depth of the electron beam).

The corresponding TEM image, given in Fig. 7, reveals a unique view of the nature of the reaction between the Hf and BN powders. Large flake-like crystals are seen having an unusual surface morphology. As labeled, the larger flakes are hexagonal BN as confirmed by both electron diffraction and EDX analysis (the latter is shown in the inset).

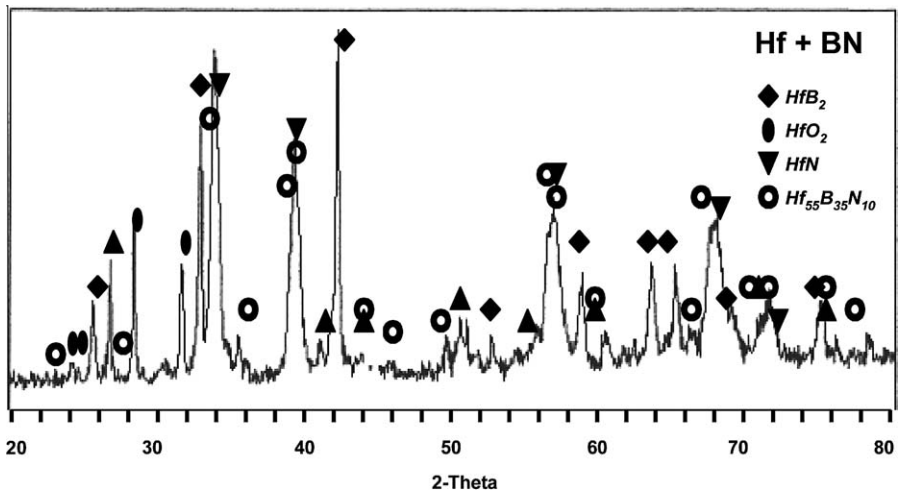

(a)

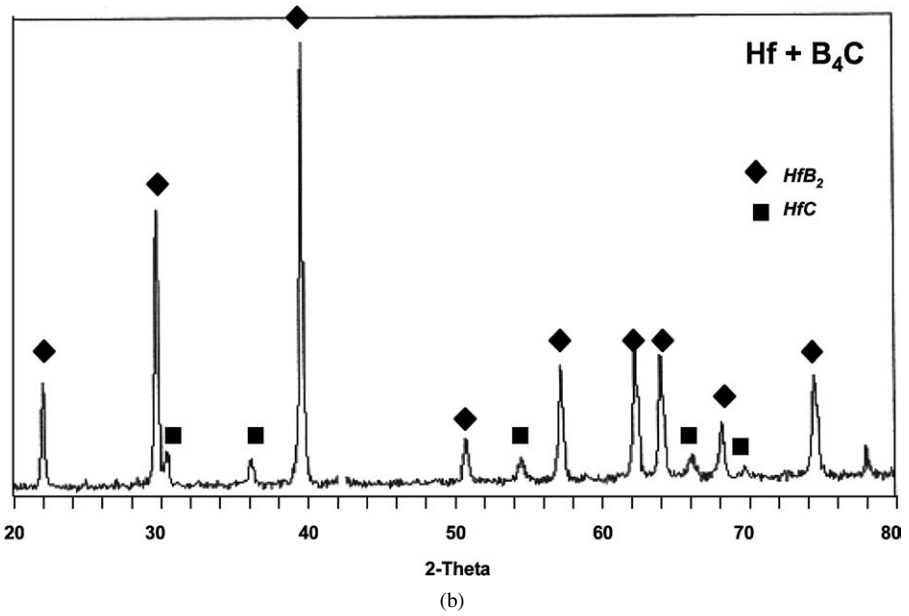

(b)

Figure 5 Reactions between Hf and solid phase compounds containing boron at 1500°C lead to the formation of HfB_2 associated with other Hf compounds such as (a) HfN in the reaction with BN and (b) HfC in the presence of B_4C.

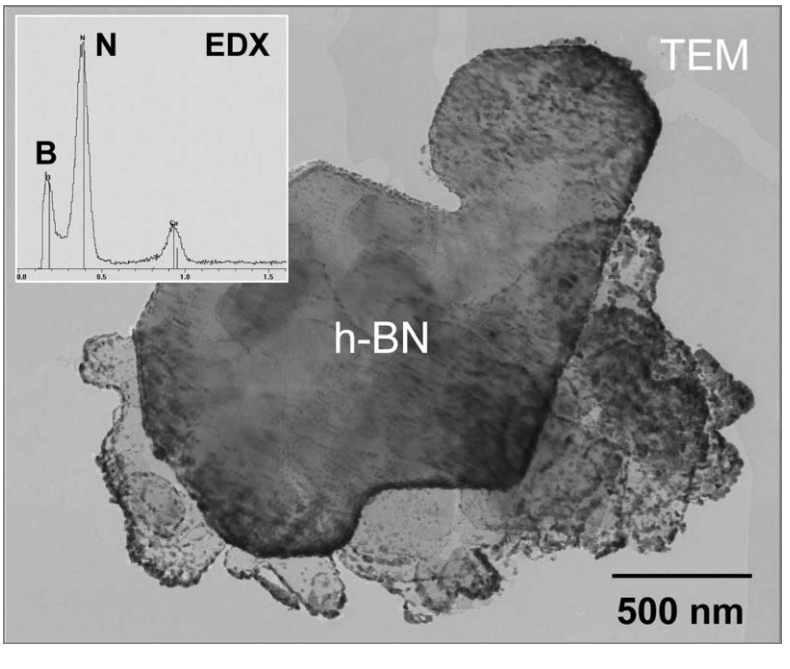

Figure 6 SEM image of the powder sample obtained via reaction (14) at 1500°C, showing a plate-like morphology of most of the particles.

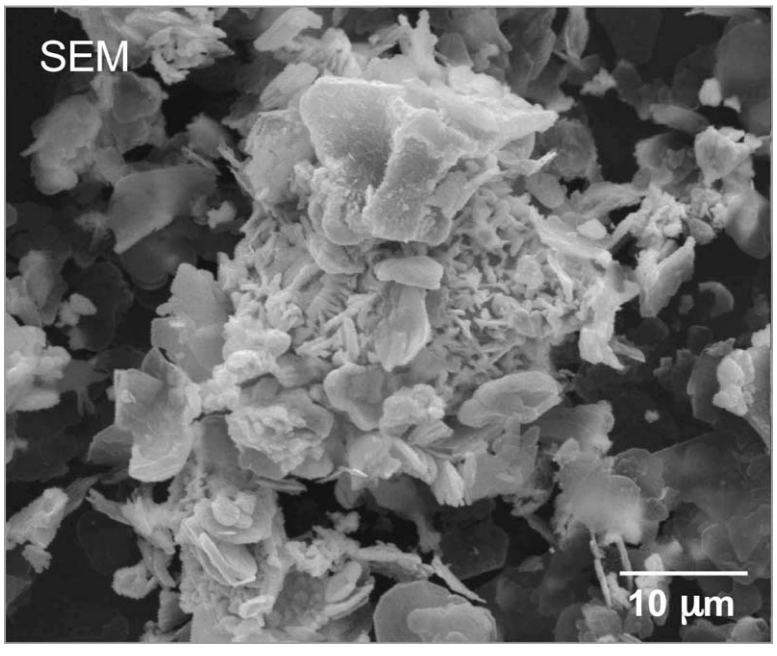

Figure 7 TEM image (corresponding to Fig. 6) of rather large BN single crystals, which revealed a "rough" surface morphology (darker regions). The inset shows the EDX analysis taken from the center of the large central BN particle.

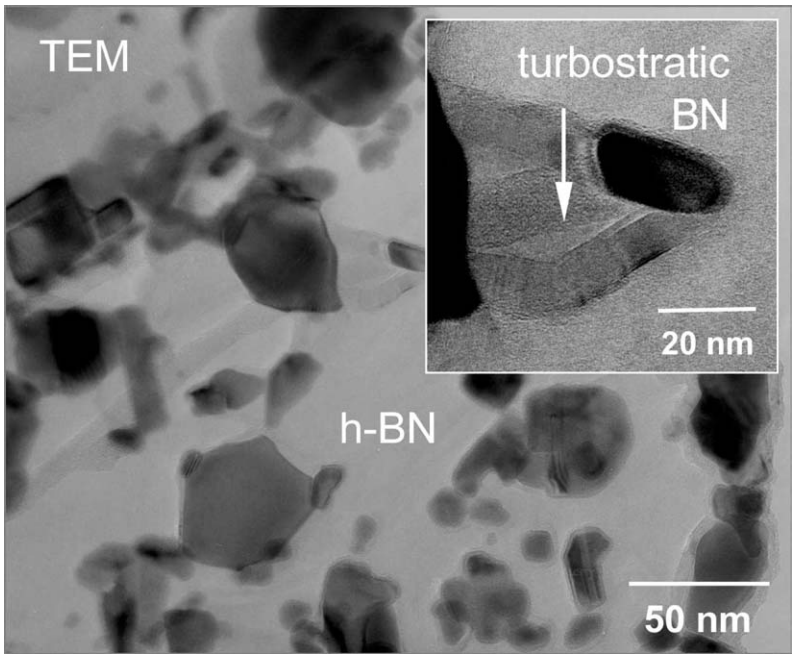

Figure 8 High-magnification TEM image of the surface area of the BN crystal shown in Fig. 7. Note that apart from the small dark particles in the surface, turbostratic BN was also observed (inset).

Imaging at higher magnification (Fig. 8) revealed that the surface of the BN particles was coated by a large number of small dark particles, which were identified by electron diffraction (Debye Scherrer rings) as a combination of HfB_2 and HfN. In addition, turbostratic features (similar to turbostratic carbon) were observed and identified as turbostratic BN, as shown in the inset.

It should be noted that some larger, rather thick and dark, particles were also observed in this sample and are most likely residual Hf-metal that did not completely react. However, this particular surface reaction observed by the TEM analysis is very intriguing and immediately leads to the question of the specific reaction path that occurs during the reaction proposed in Equation 14. More detailed SEM/TEM analysis is necessary to fully understand the reaction mechanism.

The reaction between Hf and BN in the presence of molten aluminum as a practical technique to form HfB_2/AlN composite has been reported [34]:

$$\mathrm{Hf} + \mathrm{BN} + \mathrm{Al} \longrightarrow \mathrm{HfB_2} + \mathrm{AlN} \qquad (15)$$

This reaction clearly takes advantage of the molten Al as both a strong reducing agent for the BN as well as a liquid solvent for the boron and potentially for the Hf particles as well. This theme of using molten metals as vehicles to form borides and carbides of transition metals starting from either oxides or metallic powder

reagents is well documented in the literature. The gasless reduction of oxides to form carbides and borides is known as the thermite reaction and is primarily performed in the presence of magnesium, a highly oxidative metal with a very low melting point [35]:

$$MO_2 + B_2O_3 + 5Mg \longrightarrow MB_2 + 5MgO \quad (16)$$

Al is also used in a similar manner, but it is harder to separate the Al_2O_3 from the reduced material. It is, therefore, used for the fabrication of alumina-based composites. The reaction between carbide- and boride-forming elements in molten metals was reported in the patent literature as a means to form ceramic-reinforced metal composites [36, 37]. An example for such a reaction is as follows:

$$Ti + 2B + Al \longrightarrow TiB_2 + Al \quad (17)$$

The reaction between Hf and B_4C mixed powders is another dissociative-replacement reaction that occurs below 1500°C, although it is expected to be a solid-solid reaction:

$$Hf + 1/3B_4C \longrightarrow 2/3HfB_2 + 1/3HfC \quad (18)$$

Both phases of HfB_2 and HfC are observed, although the intensity of the latter is much lower (Table II, Fig. 2b). This is another corroboration of the potential for obtaining solid-solid reactions between thermally stable powders. A marginal weight gain of 0.1 wt% may indicate the potential that the reaction mechanism is assisted by an *in situ* formation of a liquid or gas phase species.

Similarly to Fig. 6 representing Reaction (14), the SEM image of the material formed in Reaction (18) (Fig. 9) shows a large fraction of plate-like particles, although the overall particle size is somewhat smaller. In addition, small, rather spherical particles are observed, revealing a higher contrast in the backscattering imaging mode (BSE). This indicates the presence of Hf (since the BSE contrast depends on the atomic number of the compound).

The corresponding TEM image, given in Fig. 10, shows a similar feature as observed during Reaction (14); see also Figs 7 and 8.

Large flake-like particles, which were identified as B_4C single crystals (electron diffraction; see inset) are coated with very small dark particles, which were identified as a mixture of HfB_2 and HfC. It is interesting to note that here again a surface reaction took place leading to the formation of Hf-containing phases on the surface of the B_4C substrate.

Similar to the reaction between Hf-metal and BN, turbostratic features were observed. In this case, the reaction led to the formation of turbostratic carbon, which was well crystallized in some areas, as shown in Fig. 11 (Fourier-filtered HRTEM image). Fig. 11 features also a very small crystallite of a hafnium-containing product formed at the surface of the boron carbide particle.

The following reactions have been carried out to complete this set of screening the Hf-B-N-C system:

$$Hf + N_2 \longrightarrow HfN \text{ (occurs at 1200°C)} \quad (19)$$

$$HfB_2 + N_2 \longrightarrow (HfB_2) + HfN + Hf_7O_8N_4 \times (\text{weak XRD pattern}) + (BN?) \quad (20)$$

$$HfC + N_2 \longrightarrow \text{No reaction is observed by XRD} \quad (21)$$

$$HfN + C \longrightarrow HfC + (HfN) \quad (22)$$

$$HfN + 2B \longrightarrow HfB_2 + (HfN) + (BN?) \quad (23)$$

$$HfC + 2B \longrightarrow HfB_2 + (HfC) \quad (24)$$

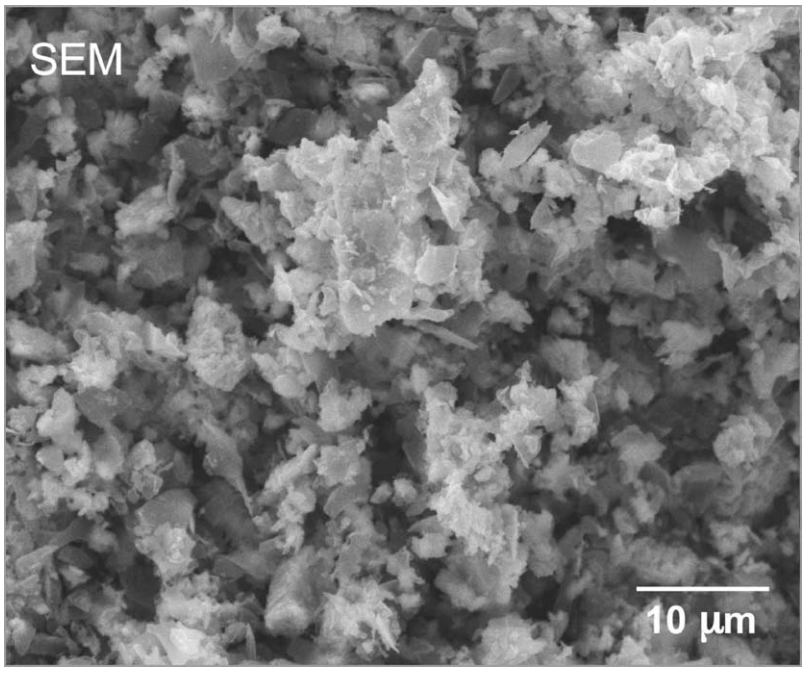

Figure 9 SEM image of the powder sample obtained via reaction (18) at 1500°C, showing predominantly plate-like particles.

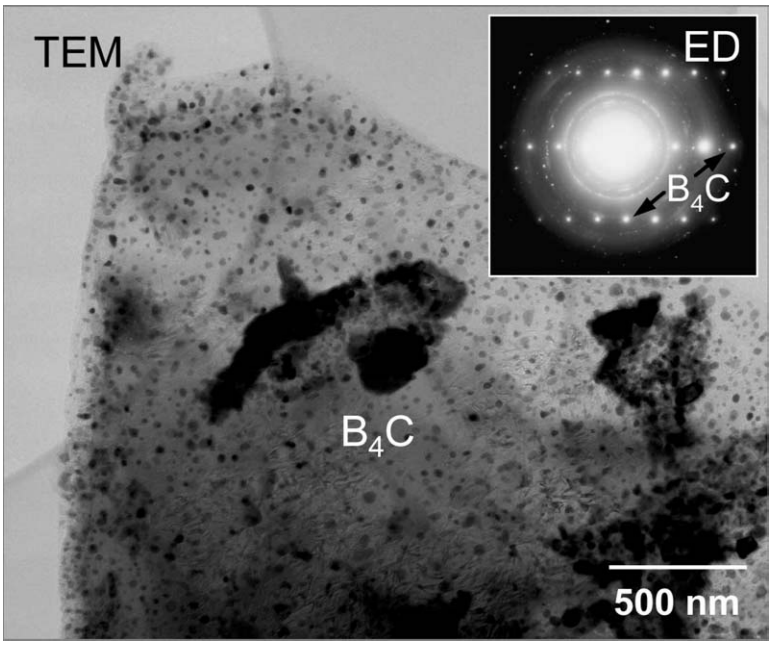

Figure 10 TEM image (corresponding to Fig. 9) showing a large single crystal of B_4C (confirmed via electron diffraction; see inset), which is coated with a high number of small dark particles.

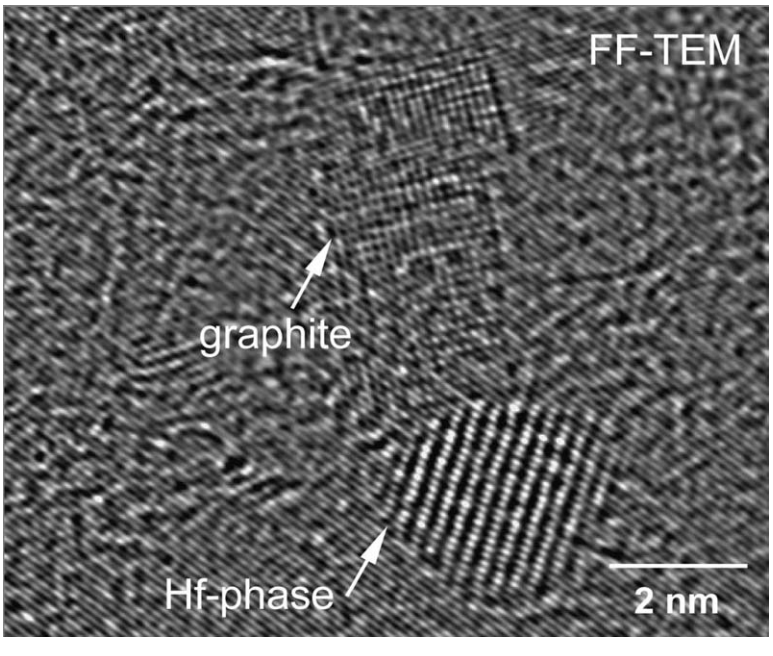

Figure 11 Fourier filtered HRTEM image showing the formation of graphitic carbon (as well as Hf-compounds—lower right corner) on the surface of the B_4C crystals (see also Fig. 10).

The results are summarized in Table V. Some of the reactions indeed occur under these conditions, representing further the likelihood for a relatively low-temperature reactivity of the system, provided that the reaction is spontaneous according to thermodynamic calculations as shown in Tables II and IV. Although the reaction between HfC and N_2 is thermodynamically favorable and gas phase interaction is involved, no reactivity has been detected. In contrast, a small conversion is observed in Equation 22, which is endothermic according to our calculations. Nevertheless, this reaction is very slow at this temperature.

The XRD analyses of reactions indicating the reactivity of the Hf-B-N-C system are assembled in Fig. 12. The absence of weight loss in Equation 23, in spite of

TABLE V Reactions involving Hf derivatives carried at 1500°C

Reactants	Weight change during heating to 1500°C (WT%)	Observed crystalline phases after heating to 1500°C (found by XRD)
$HfB_2 + N_2$	+8.2 (at 1400°C)	HfB_2 (strong) HfN (medium) $Hf_7O_8N_4$ (weak),
$Hf + N_2$	+5.7 (at 1200°C)	NA (dark golden color)
$HfC + N_2$	No change	HfC (very strong)
HfC + 2B	−0.7	HfB_2 (very strong) HfC (strong)
HfN + 2B	No change	HfB_2 (very strong) HfN (weak)
HfN + C	+0.5	HfN (strong) HfC (weak)

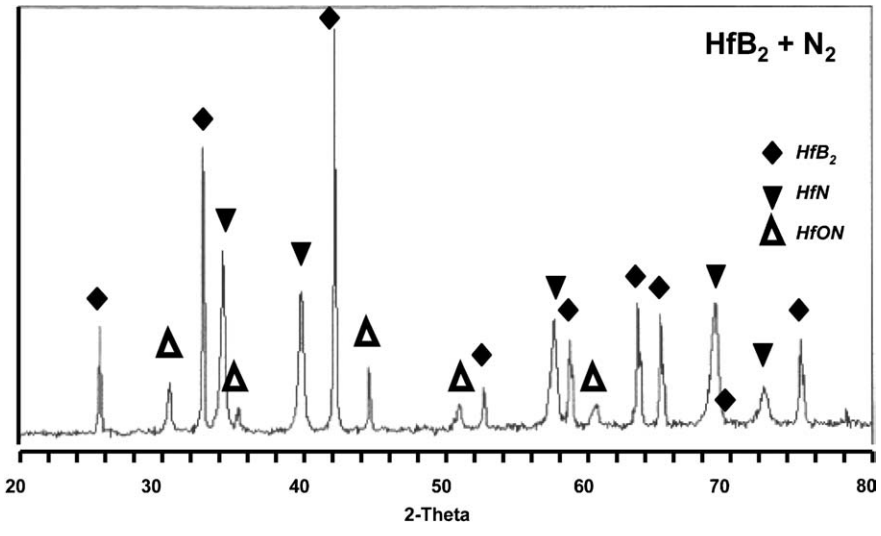

(a)

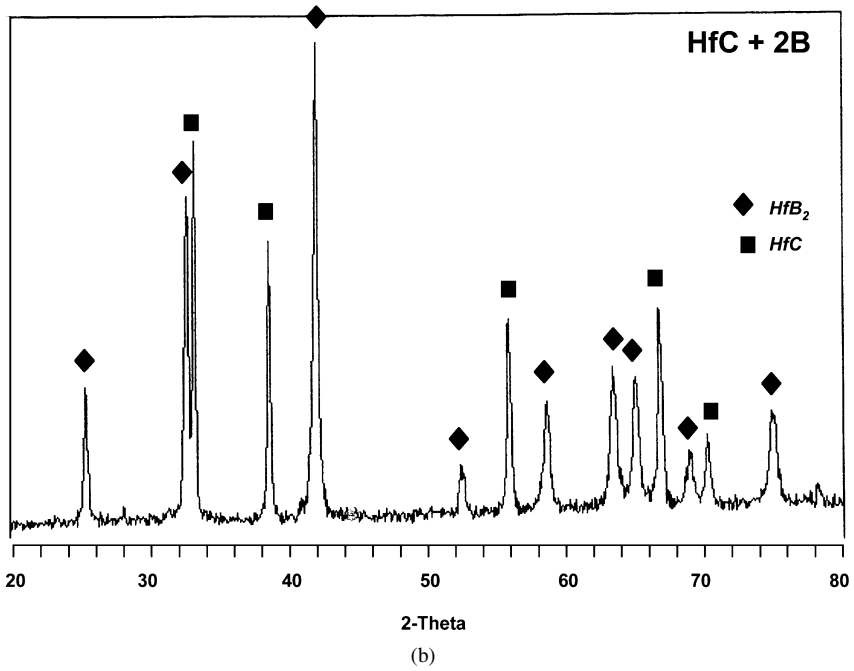

(b)

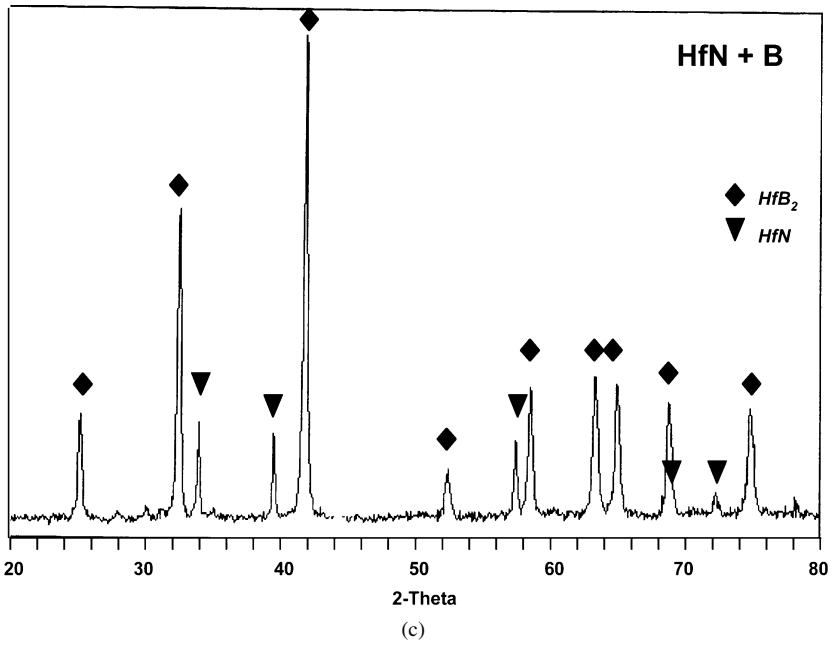

(c)

Figure 12 Reactions involving Hf compounds at 1500°C that reveal the formation of derived products: (a) $HfB_2 + N_2$; (b) HfC + B; (c) HfN + B; and (d) HfN + C.

(*Continued on next page*)

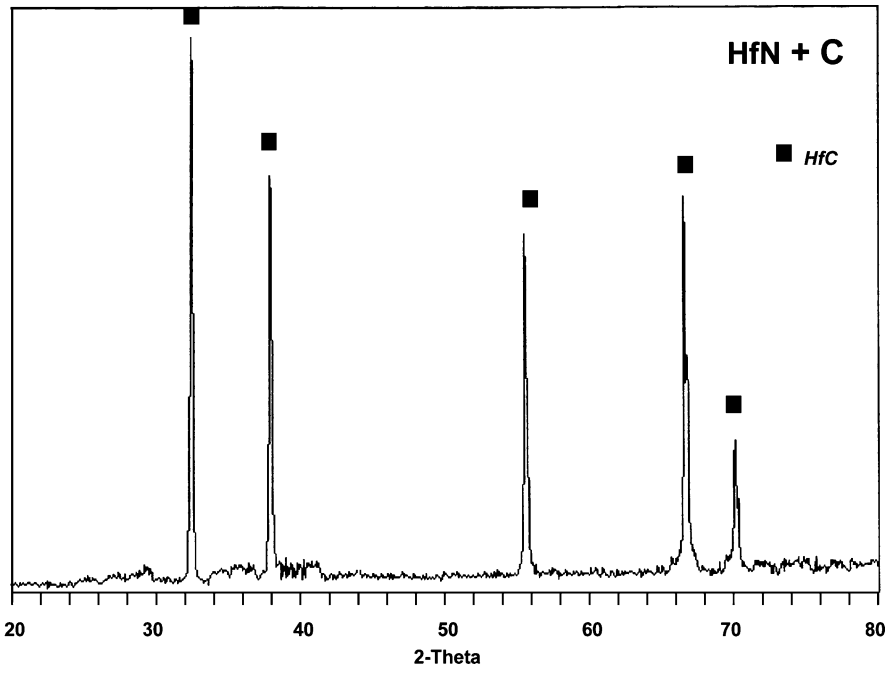

(d)

Figure 12 (*Continued*)

definite detection of crystalline products, can be explained if a dissociative reaction occurs and forms a BN phase. However, a BN phase is not found in the XRD profile of this reaction. Similarly, BN or BN-like domains may be present in the reaction products of Equations 20 and 23. However, BN was not detected by XRD.

Finally, based on Equations 2 and 18 and thermodynamic calculations, the following reaction has been performed, which is a combination of the endothermic borothermic/carbothermal reaction and the exothermic dissociative-substitution reaction:

$$\mathrm{Hf} + 1/3\mathrm{HfO_2} + 2/3\mathrm{B_4C} \longrightarrow 4/3\mathrm{HfB_2} + 2/3\mathrm{CO} + (\mathrm{HfC} + \mathrm{HfO_2}) \quad (25)$$

The reaction progresses very well but is not completed after 1 h at 1500°C according to the mass loss calculation. This reaction is devised to eliminate all the oxygen and carbon under exothermic conditions and lower the volume of gas released, in contrast to all the other carbothermal reductions discussed above. The amount of gas released is only one-quarter (or less) of the conventional carbothermal reductions forming HfB_2. Only small levels of HfO_2 and HfC are still detected by XRD. The presence of HfC suggests that Equation 18 (the exothermic reaction) occurs first and that HfC may be an intermediate product in the overall reaction. This reaction will be very useful in developing a precursor approach in further studies.

4.2. Incorporation of silicon

The investigation of low-temperature reactivities within the system of Hf-B-C-O-N is still in progress. However, for various reasons it is planned to extend this investigation and introduce also silicon chemistry into our experimental considerations. The main reason is the fact that the goal of the overall research is the processing of HfB_2/SiC composite, although the SiC is a minor fraction by volume (20%) and weight (6.4%). Interactions between these two domains and their elements should clearly be of high interest. Furthermore, Si can serve as a liquid aid for the solid-solid reactions such as discussed in the previous section, and ease the sintering and microstructure rearrangement similarly to the reactions that occur in the presence of molten Mg and Al.

The initial effort reported in this article has assessed the potential reactivity of desired elements of the system Hf-B-C in the presence of elemental Si. Table VI reveals the thermodynamic values of such potential reactions between 1000 and 1500°C, as well as reactions involving O and N.

TABLE VI Thermodynamic values of reactions involving Si in the Hf-B-Si-C-N-O system

Reaction	ΔG_{1000} (KJ/mol)	ΔH_{1000} (KJ/mol)	ΔG_{1500} (KJ/mol) (temp of $\Delta G = 0$)	ΔH_{1500} (KJ/mol)
$\mathrm{Hf} + 2\mathrm{B} + \mathrm{Si} + \mathrm{C} = \mathrm{HfB_2} + \mathrm{SiC}$	−358	−406	−336	−461
$\mathrm{Si} + \mathrm{C} = \mathrm{SiC}$	−61	−72	−55	−122
$\mathrm{HfC} + \mathrm{SiO_2} = \mathrm{HfO_2} + \mathrm{SiC}$	−91	−98	−88	−95
$\mathrm{Hf} + \mathrm{C} + \mathrm{SiO_2} = \mathrm{HfO_2} + \mathrm{SiC}$	−292	−303	−288	301
$\mathrm{SiO_2} + 3\mathrm{C} = \mathrm{SiC} + 2\mathrm{CO}$	173	601	7 (1522°C)	589
$\mathrm{Hf} + 2\mathrm{B} + \mathrm{SiO_2} + 3\mathrm{C} = \mathrm{HfB_2} + \mathrm{SiC} + 2\mathrm{CO}$	−124	268	−71	252
$\mathrm{Hf} + 1/2\mathrm{B_4C} + 1/2\mathrm{Si} = \mathrm{HfB_2} + 1/2\mathrm{SiC}$	−306	−331	−297	−360
$\mathrm{Hf} + 2\mathrm{BN} + 3/2\mathrm{Si} = \mathrm{HfB_2} + 1/2\mathrm{Si_3N_4}$	−196	−204	−189	−281
$\mathrm{Si} + 2/3\mathrm{N_2} = 1/3\mathrm{Si_3N_4}$	−115	−275	−50	−321
$\mathrm{B} + \mathrm{Si_3N_4} = \mathrm{BN} + \mathrm{Si}$	−52	−43	−58	−7

The vast majority of these potential reactions are exothermic, and some are very exothermic at the discussed temperature range, with the exception of the carbothermal reduction of silica. Therefore, it can be a very appealing approach for forming the boride-carbide composites, by forming a liquid phase similarly to the ones mentioned earlier and illustrated in Equations 15 to 17.

The dissociative reactions with boron carbide and boron nitride with Hf in the presence of Si were added to the above calculations because of earlier research for the reaction between metals and boron carbide and our findings about the low-temperature reactivity of BN in the presence of Hf.

Two other intriguing reactive processing approaches have been recently reported, which fit very well the concepts discussed in this section. Talmy *et al.* reported the formation of ZrB_2/SiC and ZrB_2/ZrC/SiC composites through the following reactive process [38]:

$$Zr + C + SiB_4 \longrightarrow ZrB_2 + SiC + ZrC \qquad (26)$$

The reaction occurred during a hot-press processing with a formulation containing powders of Zr, C, and SiB_4. This study demonstrated the capability to suppress the coarsening of the boride phase, which is a typical mode in pure boride systems, resulting in inferior properties. Formulations that did not contain the ZrC phase performed best in their oxidation resistance.

Evidence for the potential of incorporating Si to form the desired HfB_2/SiC composites is found in a recent investigation of reactive hot pressing of ZrB_2/SiC composites [39]. In this article, the following reaction has been used to form strong composites under hot-press conditions with a maximum temperature of 1900°C, which is considered a relatively low processing temperature:

$$2Zr + B_4C + Si \longrightarrow 2ZrB_2 + SiC \qquad (27)$$

A series of reactions has been performed to screen potential reactions leading to HfB_2/SiC-containing composites. In this series, several of the powder mixtures were also pressed into pellets, to obtain a first indication of the capability of this approach to form the composites under milder conditions, including the pressureless heat process. The pellet-derived monolithic products are still under evaluation.

The mixed powder reaction results are summarized in Table VII.

The reaction between HfB_2, Si, and C in the composition providing monolithic composite of 80:20 volume ratio is the most obvious experiment for incorporating Si:

$$HfB_2 + Si + C \longrightarrow HfB_2 + SiC \qquad (28)$$

In this reaction, the well-known reaction-bonded silicon carbide (RBSC) is anticipated to occur after the melting of the silicon at 1410°C. The XRD analysis in this case reveals only the pattern of HfB_2 and traces of HfO_2 (see Fig. 13a). No other phases are observed by this method. Since the pelletized product obtained after heating at 1500°C demonstrated higher integrity than the green body and pellets heated at 1000°C, it is assumed that the detection limit of the XRD apparatus is the reason for the lack of signals coming from a generated SiC phase. Indeed, when the same reaction was performed with a weight ratio of 80:20 (4.00) for the anticipated two phases, a small but sharp pattern of SiC is the additional phase shown beside the strong HfB_2 pattern, as shown in Fig. 13b.

TABLE VII Reactions capable of forming HfB_2 in the presence of Si

Reactants	Weight change (%)	XRD analysis of reactions at 1500°C
HfB_2 + Si + C (derived from polyacrylonitrile) HfB_2/SiC = 80:20 volume ratio	−3.1	HfB_2 (very strong) HfO_2 (traces)
HfB_2 + C + Si HfB_2/SiC = 80:20 weight ratio	−1.1	HfB_2 (very strong) SiC (weak)
Hf + 2B + C + Si Stoichiometric mol ratios of HfB_2/SiC	−2.1	HfB_2 (very strong) SiC (strong)
Si(Hf) + 2B + C + Si Stoichiometric mol ratios	−6.2	HfB_2 (very strong) SiC (medium)
Hf + B_4C + Si Stoichiometric mol ratios	+0.3	HfB_2 (very strong) SiC (traces)
Hf + 2BN + Si Stoichiometric mol ratios		$HfSi_2$ (very strong) HfB_2 (strong) HfN (weak) Si(weak)

The above observation prompted the experiment involving the eutectic composition of Si-Hf mixture with stoichiometric B and C. The phase diagram of the two elements indicates the formation of a eutectic solution at the weight ratio of Hf:Si 38:62 (molar ratio of 1:10.4). This composition has a melting point of 1320°C. The eutectic solution was prepared first and then reacted with C and B:

$$Si_{10.4}(Hf) + 10.4C + 2B \longrightarrow 10.4SiC + HfB_2 \qquad (29)$$

This eutectic composition is intriguing for the practical reason that it lowers the temperature at which the reactions leading to the desired compositions will be assisted by a liquid binding phase. Such a reaction should be clearly associated with the presence of an additional HfB_2 powder to achieve the desired volume ratio in the entire composite. The XRD analysis, shown in Fig. 13c, reveals a larger than anticipated intensity of the HfB_2 pattern in comparison to the pattern of the stoichiometric molar ratio. This indicates either the faster development of HfB_2 versus the SiC crystalline phase or a major difference in their relative intensities. It should be noted that the reaction was carried out at 1400°C, rather than the 1500°C used in all the other experiments. Assuming that all the reactants have been converted to the desired phases, this composite possesses a weight ratio of 1.0:0.5 for HfB_2:SiC and a respective volume ratio of 10:90. The XRD pattern in Fig. 13c shows a very similar intensity for the HfB_2 and SiC phases. Comparison

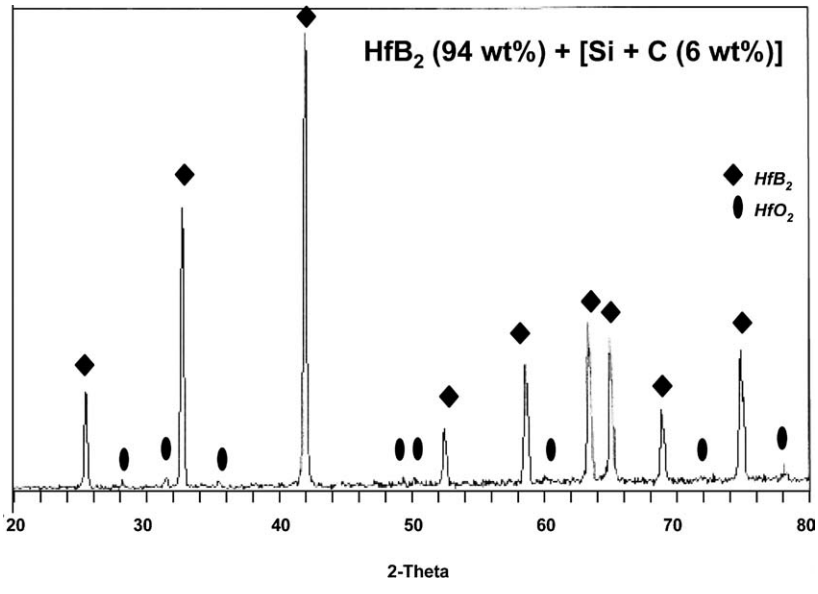

(a)

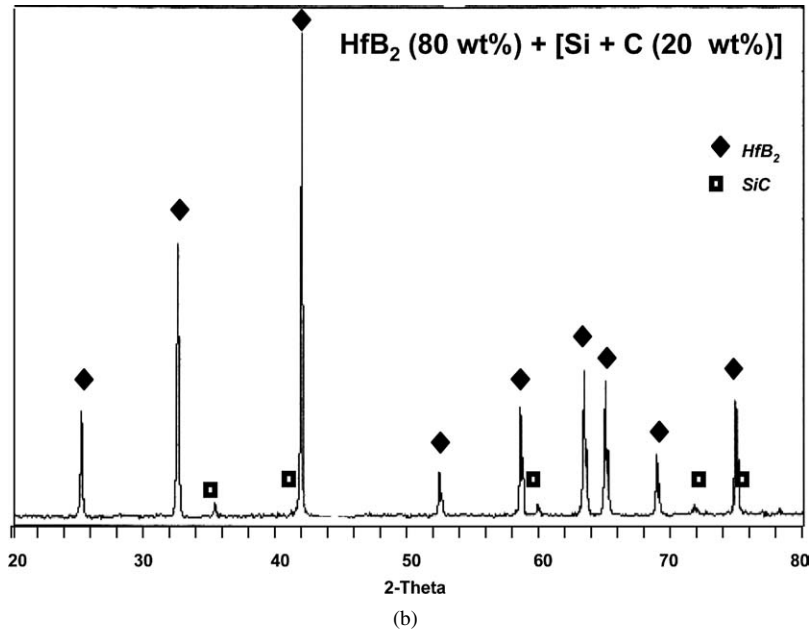

(b)

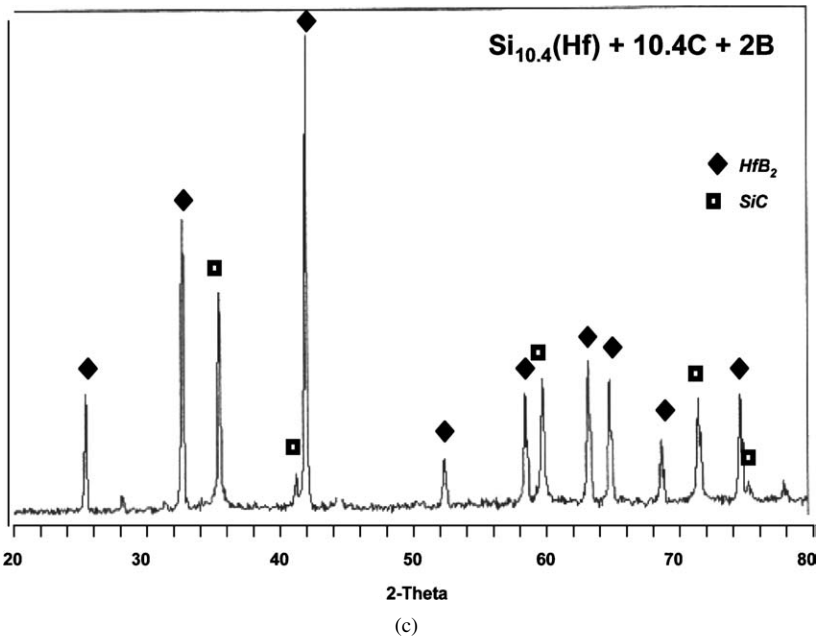

(c)

Figure 13 Reactions forming HB_2/SiC composite powders: (a) HfB_2 (94 wt%) + Si + C (6 wt%); (b) HfB_2 (80 wt%) + [Si + C (20 wt%)]; (c) $Si_{10.4}$(Hf) + 10.4C + 2B; (d) 10.4Si+ 10.4C + Hf) + 2B. (*Continued on next page*)

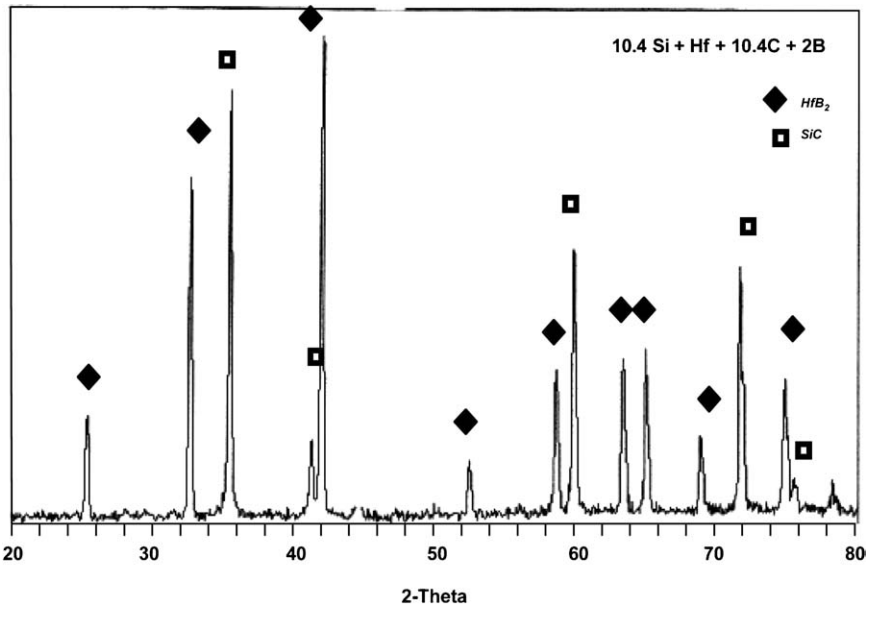

(d)

Figure 13 (*Continued*)

with the intensities shown in Fig. 13b may explain the very small pattern of SiC relative to HfB_2 as observed in Fig. 13b, indicating much lower intensity for the XRD patterns of SiC versus HfB_2.

For comparison purposes, a similar reaction with the same molar ratios was carried out for all the elements presented in the desired composite:

$$Hf + 2B + 10.3Si + 10.3C \longrightarrow HfB_2 + 10.3SiC \quad (30)$$

Holt and Munir have reported forming heterogeneous TiB_2 pellets surrounding a SiC internal pellet by pressing a core of mixed Si and C and surrounding it with a compacted powder mixture of Ti and B [40]. The heat generated by the combustion formation of the external TiB_2 was enough to form a fused SiC core. The reaction presented in Equation 30 provides the first example of the potential for forming other phases, anticipated once various polymeric precursors are incorporated, consisting of combinations of the elements Hf, Si, B, and C, blended at the atomic and molecular level. Strong and sharp patterns of HB_2 and SiC, evolved at 1500°C, are the only phases revealed by the XRD analysis (Fig. 13d). The slightly higher intensity of SiC obtained by Equation 29 relative to that obtained in Equation 30 may suggest further crystallization of SiC due to the higher reaction temperature or better capability to develop the HfB_2 phase in the eutectic situation. This system of Hf-B-Si-C-N is currently under further detailed analysis.

Two other reactions in the presence of elemental silicon have been performed based on the reported reactions that are shown by Equations 15 and 27 and discussed above. These are the anticipated dissociative reactions of Hf with either BN or B_4C in the presence of molten Si. The amount of added silicon was adjusted to the molar equivalent required to consume the carbon (in the case of using B_4C) and nitrogen (in the case of using BN). The reaction with B_4C yielded the anticipated phases according to XRD analysis:

$$Hf + B_4C + Si \longrightarrow HfB_2 + SiC \quad (31)$$

In contrast to the reaction without the presence of silicon, the HfC phase has not been observed (Equation 18). A similar reaction with BN reveals completely different reactivity and also varies from the reported reaction in the presence of molten Al (Equation 15):

$$Hf + BN + Si \longrightarrow HfSi_2 + HfB_2 + HfN + (Si) \quad (32)$$

This is the only reaction containing Si in the study, thus far, in which a strong silicide pattern and presence of crystalline Si have been detected by XRD analysis.

5. Conclusions

The screening study reported in this article reveals that the chemistry of powders from the system Hf-B-C-N and Hf-B-Si-C-N is very rich and reactive, and that numerous reactions occur at temperatures below 1500°C. Reactions of loosely mixed powders proceed in spite of the very high thermal stability of Hf compounds, as manifested by extremely high melting points and lack of phase transformations at elevated temperature. In particular, they are not expected to occur as solid-solid phase reactions in the absence of gaseous or liquid phase facilitation. Yet, thermodynamically, such reactivities can be favorable, while the well-known carbothermal reductions are endothermic. Therefore, reactivity similar to combustion synthesis and SHS can be anticipated.

Early experimental study of powders generated by reactions with Hf metal using SEM and TEM indicates that the formation of HfB_2 and/or HfN seems to follow

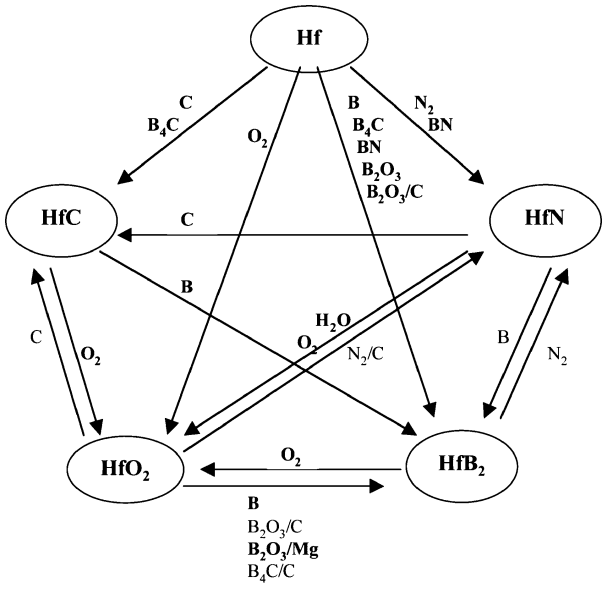

Figure 14 Reactions within the system of Hf-B-C-N-O reported or found in this study. Reactions with reagents marked in bold letters proceed (at least partially) at 1500°C or below. The rest require higher temperatures. Additional reaction products within each of the reactions (if present) are omitted.

a more complex reaction path and evidence for the formation of nanoscale "droplets" containing Hf at the surface of the boron-containing reactants. In particular, the observed surface reactions on both BN and B_4C crystal facets are very intriguing and should reflect on the specific reaction mechanisms. Local gas- or liquid-phase formation should be considered for the unexpected surface structures observed during reactions such as (14) and (18), because the Hf metal is introduced to the reaction mixture as relatively large and crude particles (median size of 4.56 μm and range of 0.3 to 20 μm).

Fig. 14 summarizes the broad range of reactions that were found to occur at 1500°C and below for the Hf-B-C-N-O system combined with other reported reactions. Many reactions with either elemental Hf or all of its derivatives lead to the formation of HfB_2. Of them, only the carbothermal and borothermic reactions may require temperatures higher than 1500°C to take place.

The incorporation of silicon can aid the Hf reactivities by forming a liquid phase at 1410°C or below and also scavenge excess carbon to form the desired SiC phase. This series of reactions is not yet completed. However, our current evaluation indicates that the formation of HfB_2 and SiC phases seems to be predominant in many of the reactions, which can be used as part of the desired composite processing under milder conditions than currently practiced.

The reactions illustrated in Fig. 14 should be considered during the design and development of any practical precursor technology. They provide much more flexibility in using combinations of polymeric precursors and reactive powders. They can either provide the formation of a binding phase, molten aids to promote reactivity, and released energy to support other endothermic reactions *in-situ*, or lead to a cascade of intermediate reactions leading to the desired phases and microstructures.

Acknowledgments

This work was funded by AFOSR and performed under Contract F49620-03-C-0026. Special thanks are given to Dr. Joan Fuller of AFOSR for her support in promoting better understanding of UHTC systems.

References

1. I. E. CAMPBELL and E. M. SHERWOOD, "High-Temperature Materials and Technology" (Wiley, New York, 1967).
2. J. B. BERKOWITZ-MATTUCK, (a) *J. Electrochem. Soc.* **113** (1966) 908. (b) J. B. BERKOWITZ-MATTUCK, *J. Electrochem. Soc.* **114** (1967) 1030.
3. W. C. TRIPP and H. C. GRAHAM, *J. Electrochem. Soc., Solid State Sci.* **118**(7) (1971) 1195.
4. R. A. CUTLER, "Engineering Properties of Borides in Engineering Materials Handbook," Ceramics and Glasses, ASM International, Metals Park, Ohio (1987) Vol. 4.
5. E. L. COURTRIGHT, H. C. GRAHAM, A. P. KATZ and R. J. KERANS, "Ultrahigh Temperature Assessment Study of Ceramic Matrix Composites," Report No. WL-TR-91-4061, Wright-Patterson AFB, Ohio (1991).
6. C. B. BARGERON, R. C. BENSON, R. W. NEWMAN, A. N. JETTE and T. E. PHILLIPS, *Johns Hopkins APL Tech. Dig.* **14**(1) (1993) 293.
7. K. UPADHYA, J. M. YANG and W. HOFFMAN, *Amer. Ceram. Soc. Bull.* **76**(12) (1997).
8. W. C. TRIPP, H. H. DAVIS and H. C. GRAHAM, *ibid.* **52** (1973) 612.
9. M. M. OPEKA, I. G. TALMY, E. J. WUCHINA, J. A. ZAYKOSKI and S. J. CAUSEY, *J. Eur. Ceram. Soc.* **19** (1999) 2405.
10. L. KAUFMAN, "Boride Composites—A New Generation of Nose Cap and Leading Edge Materials for Reusable Lifting Re-entry Systems," AIAA Paper No. 70-278, AIAA Advanced Space Transportation Meeting (Feb. 1970).
11. J. D. BULL, D. J. RASKY and C. J. C. KARIKA, in Proceedings of the 24th International SAMPE Technical Conference (1992) p. 1092.
12. J. BULL, M. J. WHITE and L. KAUFMAN, U.S. Patent 5,750,450 (May 12, 1998).
13. L. KAUFMAN, AFML Report No. RTD-TDR-63-4096, Part II (Feb. 1965).
14. *Idem.*, NSWC Report No. TR 86-242 (June 1986).
15. (a) E. RUDY and ST. WINDISCH, U.S. Air Force Tech. Doc. Report AFML-TR-65-2, Part 1, Vol. IX (Feb. 1966), p. 1. (b) E. RUDY and J. PROGULSKI, *Planseeber Pulvermet.* **15** (1967) 13.
16. W. D. KINGERY, H. K. BOWEN and D. R. UHLMANN, "Introduction to Ceramics" (Wiley & Sons, New York 1976) Chapt. 10.
17. M. D. SACKS, N. BOZKURT, and G. W. SCHEIFELE, *J. Amer. Ceram. Soc.* **74**(10) (1991) 2428.
18. M. D. SACKS, Y.-J. LIN, G. W. SCHEIFELE, K. WANG and N. BOZKURT, *ibid.* **78**(11) (1995) 2897.
19. G. A. ZANK, (a) U.S. Patent 5,449,646 (Sept. 12, 1995); (b) U.S. Patent 5,527,748 (June 18, 1996).
20. Z. A. MUNIR and U. ANSELMI-TAMBURINI, *Mater. Sci. Reports* **3** (1989) 277.
21. A. W. WEIMER, "Carbide, Nitride and Boride Materials Synthesis and Processing" (Chapman & Hall, London 1997) p. 79.
22. V. I. MATKOVICH, "Boron and Refractory Borides" (Springer-Verlag, Heidelberg, 1977).
23. I. P. BOROVINSKAYA, A. G. MERZHANOV, N. P. NOVIKOV and A. K. FILONEKO. *Fiz. Gor. Vzryva* **10** (1974) 4.
24. Z. A. MUNIR, private communication (2003).
25. V. V. ALEKSANDROV and M. A. KORCHAGIN, *Fiz. Gor. Vzryva* **23** (1987) 55.
26. J. KIM and C. H. MCMURTHY, *Ceram. Eng. Sci. Proc.* **6** (1985) 1313.
27. J. J. K. WALKER, *Adv. Ceram. Mater.* **3** (1988) 601.

28. H. ZHAO, Y. HE and Z. JIN, *J. Amer. Ceram. Soc.* **78** (1995) 2534.
29. A. W. WEIMER, W. G. MOORE, R. P. ROACH, J. E. HITT and E. S. E. PRATSINIS, *ibid.* **75** (1992) 2509.
30. Z. HU, M. D. SACKS, G. A. STAAB, C.-A. WANG and A. JAIN, in Ceramic Engineering and Science Proceedings, edited by H.-T. Lin and M. Singh **23**(4) (2002) 711.
31. N. P. NOVIKOV, I. P. BOROVINSKAYA and A. G. MERZHANOV, in "Combustion Processes in Chemical Technology and Metallurgy," edited by A. G. Merzhanov (Chernogolovka, Moscow, 1975) p. 174.
32. A. B. AVAKYAN, A. R. BAGRAMYAN, I. P. BOROVINSKAYA, S. L. GRIGORYAN and A. G. MERZHANOV, in "Combustion Processes in Chemical Technology and Metallurgy," edited by A. G. Merzhanov (Chernogolovka, Moscow, 1975) p. 174.
33. R. H. LAMOREAUX, D. L. HIDENBRAND and L. BREWER, *J. Phys. Chem.* **16** (1987) 419.
34. M. KOBASHI and N. TONOKURA, *Keikinzoku* **46** (1996) 638.
35. A. G. MERZHANOV, in "Combustion and Plasma Synthesis of High-Temperature Materials," edited by Z. A. Munir and J. B. Holt (VCH Publishers, New York, 1990) p. 1.
36. J. M. BRUPBACHER, L. CHRISTODOULOU and D. C. NAGLE, U.S. Patent 4,710,348 (1987).
37. *Idem.*, U.S. Patent 4,915,903 (1990).
38. I. G. TALMY, J. A. ZAYKOSKI and M. A. OPEKA, *Ceram. Eng. Sci. Proc.* **19**(3) (1998) 105.
39. G. J. ZHANG, Z. Y. DENG, N. KONDO, J. F. YANG and T. OHJI, *J. Amer. Ceram. Soc.* **83**(9) (2000) 2330.
40. J. B. HOLT and Z. A. MUNIR, in Proceedings of 1st International Symposium on Ceramic Components for Engines, edited by S. Somiya, E. Kanai and K. Ando (KTK Scientific Publishers, Tokyo, 1983) p. 721.

Received 16 October 2003
and accepted 22 March 2004